# Selective Antitumor Effect of Novel Protease-Mediated Photodynamic Agent

**Yongdoo Choi, Ralph Weissleder, and Ching-Hsuan Tung**

Center for Molecular Imaging Research, Massachusetts General Hospital, Harvard Medical School, Charlestown, Massachusetts

## Abstract

**A new approach to selective photodynamic therapy (PDT) was developed by designing chlorin e6 (Ce6)–containing macromolecules, which are sensitive to tumor-associated proteases. The agents are nontoxic in their native state but become fluorescent and produce singlet oxygen on protease conversion. Coupled with optimized delivery systems, we show that (*a*) the agents efficiently accumulate in tumors due to the enhanced permeability and retention effect, (*b*) the agents are locally activated by proteases, (*c*) local drug concentrations can be measured by quantitative fluorescence tomography, and (*d*) light-treated tumors show reduced growth. A single low dose of PDT (0.125 mg Ce6 equivalent/kg) was sufficient to suppress tumor growth by >50%. Activatable singlet oxygen generation agents provide increased efficacy with reduced toxicity, and it could become a powerful PDT.** (Cancer Res 2006; 66(14): 7225-9)

## Introduction

Photodynamic therapy (PDT) using combinations of chemical photosensitizers and light has been used successfully to treat cancers and other nonmalignant conditions (1). Typical photosensitizers are designed to be nontoxic to cells in the absence of light. When illuminated by an appropriate wavelength, the excited photosensitizer transfers its energy to neighboring molecular oxygen, producing cytotoxic singlet oxygen, which causes selective damage to tissues *in situ*. Despite significant advantages of PDT over the conventional chemotherapy, limited tumor selectivity of PDT agents has remained major obstacles. In addition, phototoxicity to skin and eyes is a considerable limitation of existing agents (1). In the current study, we developed a new strategy termed protease-mediated PDT (PM-PDT). This was achieved by constructing PDT agents that are "activatable" by tumor-associated proteases.

Tumor-associated proteases are known to function at multiple stages of tumor progression, affecting tumor establishment, growth, neovascularization, intravasation, extravasation, and metastasis (2–5). Prior reports have shown that several proteases (e.g., cathepsins and matrix metalloproteinases) are up-regulated in many cancer types (6–8), and potentially, these tumor-associated proteases could act as activators of the proposed PM-PDT agent.

Porphyrin-based photosensitizers have been shown previously to exhibit reduced fluorescence and singlet oxygen generation (SOG) on aggregation (9–11). Based on this observation, we coupled multiple chlorin e6 (Ce6) molecules onto a biodegradable poly-L-lysine grafted with monomethoxy-polyethylene glycol (PEG; L-PGC) to induce aggregation and self-quenching (Fig. 1) while still representing a biocompatible agent with favorable tumor-accumulating properties (12). Previously, we have used analogous backbones to synthesize protease activatable imaging probes (13). We hypothesized that the high local density of Ce6 causes quenching (i.e., low fluorescence and low SOG). Fluorescence and SOG are expected to increase on protease-mediated release of the photosensitizers.

## Materials and Methods

**Synthesis of L-SR15 and D-SR16.** L-PGC (average molecular weight, 375 kDa) and D-PGC (average molecular weight, 344 kDa) were purchased from VisEn Medical, Inc. (Woburn, MA). L-PGC consists of poly-L-lysine (48 kDa) backbone grafted with monomethoxy-PEG (5 kDa, percent PEGylation, 30%). D-PGC consists of poly-D-lysine (44 kDa) grafted with PEG (percent PEGylation, 28%). The conjugation of Ce6 (Frontier Scientific, Logan, UT) to lysine residues in the PGC backbone was done using 1-ethyl-3-(3-dimethylaminopropyl)carbodiimide HCl (EDC) as a coupling agent. In brief, total 1.7 mL mixture solutions, consisting of 1,140 μL of 9 μmol/L L-PGC or D-PGC in distilled water, 423 μL of 1.8 mmol/L Ce6 in 33 mmol/L $Na_2HPO_4$, and 120 μL of 13 mmol/L EDC in distilled water, were added into microcentrifuge tubes and gently shaken at 25°C in the dark for 20 hours. After reaction, the conjugates were purified by size exclusion chromatography (Bio-Gel P-10 gel, Bio-Rad, Hercules, CA) using 10 mmol/L phosphate buffer (pH 7.4) as an eluent. The substitution ratio of Ce6 on each PGC chains was determined by measuring the absorbance at 400 nm of conjugates dissolved in 0.1 mol/L NaOH/0.1% SDS and calculating the amount of Ce6 present using $\varepsilon_{400nm}$ = 150,000 (11). The substitution ratio (i.e., the number of Ce6 attached to each PGC chain) was 15 for L-PGC conjugate (L-SR15) and 16 for D-PGC conjugate (D-SR16), respectively.

**Enzyme activation of fluorescence signal and SOG.** Enzymatic activation of the conjugates by cathepsin B was tested as following: L-SR15 or D-SR16 (0.84 nmol Ce6 eq.) dissolved in 34 μL sodium acetate buffer [20 mmol/L sodium acetate, 1 mmol/L EDTA, 1 mmol/L DTT (pH 5.0)] was mixed with 0.2 nmol cathepsin B (8 μL in sodium acetate buffer, human liver, Calbiochem, La Jolla, CA) for the enzyme-treated sample or equal volume of sodium acetate buffer (8 μL) for the buffer-treated sample. The mixture was then incubated at 37°C for 22 hours. To compare enzymatic cleavage of L-SR15 conjugate by cathepsins, identical molar amounts of cathepsin L (human liver, Calbiochem) or cathepsin S (human spleen, Calbiochem) were incubated with the conjugate using identical conditions as described above.

For samples treated with a specific cathepsin B inhibitor CA-074 (Peptide International, Louisville, KY), 0.2 nmol cathepsin B (8 μL) was incubated with 1 mmol/L CA-074 (8 μL) in 20 mmol/L sodium acetate buffer (pH 5.0) at room temperature for 10 minutes. Then, L-SR15 or D-SR16 (0.8 nmol Ce6 eq.) dissolved in 26 μL sodium acetate buffer [20 mmol/L sodium acetate, 1 mmol/L EDTA, 1 mmol/L DTT (pH 5.0)] was added into CA-074-pretreated cathepsin B solution and incubated at 37°C for 22 hours. Before measuring fluorescence intensities of the samples, 160 μL phosphate buffer [10 mmol/L phosphate, 140 mmol/L NaCl, 3 mmol/L KCl (pH 7.4)] was

**Requests for reprints:** Ching-Hsuan Tung, Center for Molecular Imaging Research, Massachusetts General Hospital, Harvard Medical School, 149, 13th Street, Room 5406, Charlestown, MA 02129. Phone: 617-726-5779; Fax: 617-726-5708; E-mail: tung@helix.mgh.harvard.edu.



doi:10.1158/0008-5472.CAN-06-0448

added to each sample. Thereafter, emission (excitation, 650 nm) was recorded at 670 nm using a computer-controlled fluorescence plate reader (Safire II, Tecan, Durham, NC).

Bleaching of *N,N*-dimethyl-4-nitrosoaniline (RNO) was used as an indicator for photo-induced singlet oxygen in the presence of histidine as a chemical trap for singlet oxygen (14). In brief, the sample solution used in the fluorescence measurement was prepared by mixing 480 μL RNO solution [20 mmol/L phosphate, 20 mmol/L histidine, 100 μmol/L RNO (pH 7.0)]. The mixture was added into a UV quartz cell and irradiated with light at a dose rate of 41.4 mW/cm$^2$ at 650 nm. At 0 minute and every 2 minutes of light treatment, solutions were mixed by pipetting and transferred to the UV spectrophotometer. The bleaching of RNO was measured at 440 nm. SOG was calculated from the initial slope of the RNO variation versus irradiation time. SOG of free Ce6 was measured at the same condition, which was used for the conjugates. Relative values of SOG of the conjugates compared with free Ce6 equal to the slope of unknown samples divided by the mean slope of free Ce6. All experiments were done in triplicate.

***In vivo* PDT.** All animal studies were approved by the Institutional Animal Care Committee. HT1080 (human fibrosarcoma) obtained from American Type Culture Collection (Manassas, VA) were maintained in DMEM (Cellgro, Washington, DC) supplemented with 10% fetal bovine serum (Cellgro) and 1% penicillin/streptomycin at 37°C in humidified atmosphere with 5% $CO_2$. Female athymic nude mice (*nu/nu*, 6-7 weeks old, 21-23 g) were purchased from Charles River (Wilmington, MA). HT1080 cell line ($1.5 \times 10^6$ cells/0.05 mL DMEM) was implanted s.c. into both hind legs of each mouse. When the tumors reached 3 to 5 mm in diameter, a total of 70 healthy mice (8 mice for fluorescence imaging, 15 mice for apoptosis study, and 47 mice for tumor growth) were randomly divided into five groups. L-SR15 or D-SR16 was dissolved in sterilized PBS [10 mmol/L, 140 mmol/L NaCl, 3 mmol/L KCl (pH 7.4)] at a concentration of 35.7 μmol/L, respectively. Mice in groups 1 and 2 received i.v. injection of either L-SR15 (group 1, 16 mice) or D-SR16 (group 2, 16 mice) at the dose of 0.125 mg Ce6 equivalent/kg. One day after drug injection, mice were treated with light using a diode laser at 650 nm to give dose of 10 J/cm$^2$ at an irradiance of 42 mW/cm$^2$, and light spot diameter was 1 cm. Eight mice in group 3 received i.v. injection of L-SR15 at the same dose but were not treated with light. Mice in groups 4 and 5 received i.v. injection of either free Ce6 (0.125 mg/kg, 15 mice in group 4) or sterilized PBS (140 μL/mouse, 15 mice in group 5) followed by light treatment at 24 hours postinjection.

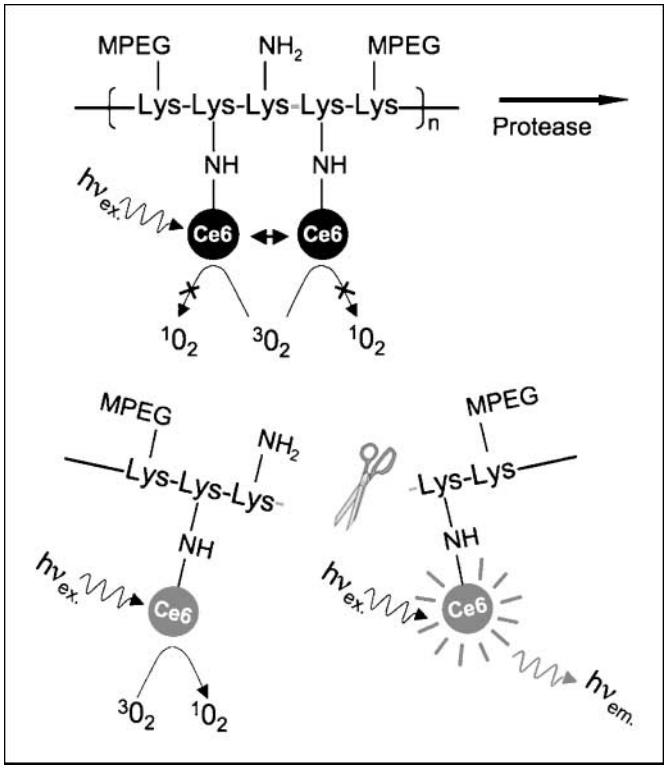


**Figure 1.** Schematic diagram of PM-PDT strategy. Fluorescence and SOG is quenched due to energy transfer between Ce6 molecules. Following proteolytic cleavage of the peptide backbone, released Ce6 regains its fluorescent properties and SOG on light excitation.

The day of photosensitizer injection was considered as day 0 and tumor volumes of the mice were measured periodically at days 0, 1, 4, 6, and 9. Tumor volume was calculated using the formula: 1/2 × length × width × height (15). To observe the enzymatic activation of L-SR15 in tumor tissues, tumors from eight mice were collected by sampling two mice from each of the groups 1, 2, 4, and 5 after 24 hours of i.v. injection of buffer or PGC conjugate solution. These mice did not receive light treatment. Collected tumors were snap frozen in liquid nitrogen, cut into 7 μm sections, air-dried, and mounted on slides. Mounting medium (Vectashield, Vector Laboratories, Burlingame, CA) with 4′,6-diamidino-2-phenylindole (DAPI) was used to counter stain nuclei of the tumor sections. Sections were viewed by fluorescence microscopy (Nikon Eclipse 80i, Nikon, Melville, NY).

To investigate tissue damage after PDT, tumor tissues from 15 mice were collected by sampling 3 mice from each of the groups 1 to 5 at 24 hours after PDT. Tumors were snap frozen in liquid nitrogen, cut into 7 μm sections, air-dried, and stained using the terminal deoxynucleotidyl transferase–mediated dUTP nick end labeling (TUNEL) technique with the ApopTag kit (Chemicon, Temecula, CA). Normal or apoptotic nuclei were stained as green or brown, respectively.

**Fluorescence molecular tomography.** Fluorescence molecular tomography (FMT) experiments were done using a commercially available imaging system (FMT-Solaris; VisEn Medical). Three mice (total of six tumors) were used for FMT imaging. These mice received i.v. injection of L-SR15 (0.125 mg Ce6 eq./kg) and were imaged at 24 hours postinjection. The images were acquired with 680 nm excitation laser and 715 nm emission (bandwidth, 30 nm). Briefly, objects were positioned in the imaging chamber and surrounded by matching fluid composed of 1% Intralipid (Fresenius, Melsungen, Germany) and 0.5% ink, which closely matched the optical properties of tissues. During FMT image acquisition, only the lower half of the mouse was imagined. Following data reconstruction of the entire field of view, regions of interest are selected in all three planes of view (*X, Y, Z*) and a volume of interest is generated. Image data sets were reconstructed using a normalized Born forward model adapted to small mouse models (16, 17). Details of the algorithm have been published before (17). Image acquisition time per animal was 3 to 5 minutes and reconstruction time was 1 to 3 minutes. Images were displayed as raw data sets (excitation, emission, and masks) and as reconstructed three-dimensional data sets in axial, sagittal, and coronal planes. Fluorochrome concentration in the target was automatically calculated from reconstructed images and expressed as femtomole fluorochrome/defined target volume.

**Statistical analysis.** Mean ± SD values were used for the expression of data if there is no mention about that. Statistical analyses of data were done using Student's *t* test. Differences of $P < 0.05$ were considered statistically significant.

## Results and Discussion

Following initial optimization experiments, a preparation with 15 Ce6 molecules per L-PGC molecule (L-SR15) was chosen for subsequent studies. L-SR15 showed an 86% decrease in fluorescence compared with that of free Ce6. L-PGC is a known substrate for cysteine protease (12); therefore, L-SR15 was tested against several cysteine proteases, including cathepsins B, L, and S, at pH 5.0. Among these three proteases, cathepsin B induced the highest fluorescence (Fig. 2*A*). L-SR15 treated with cathepsin B or L showed 4.0 ($P = 0.0007$) or 1.6 ($P = 0.0012$) times higher fluorescence intensities compared with control (buffer-treated L-SR15).

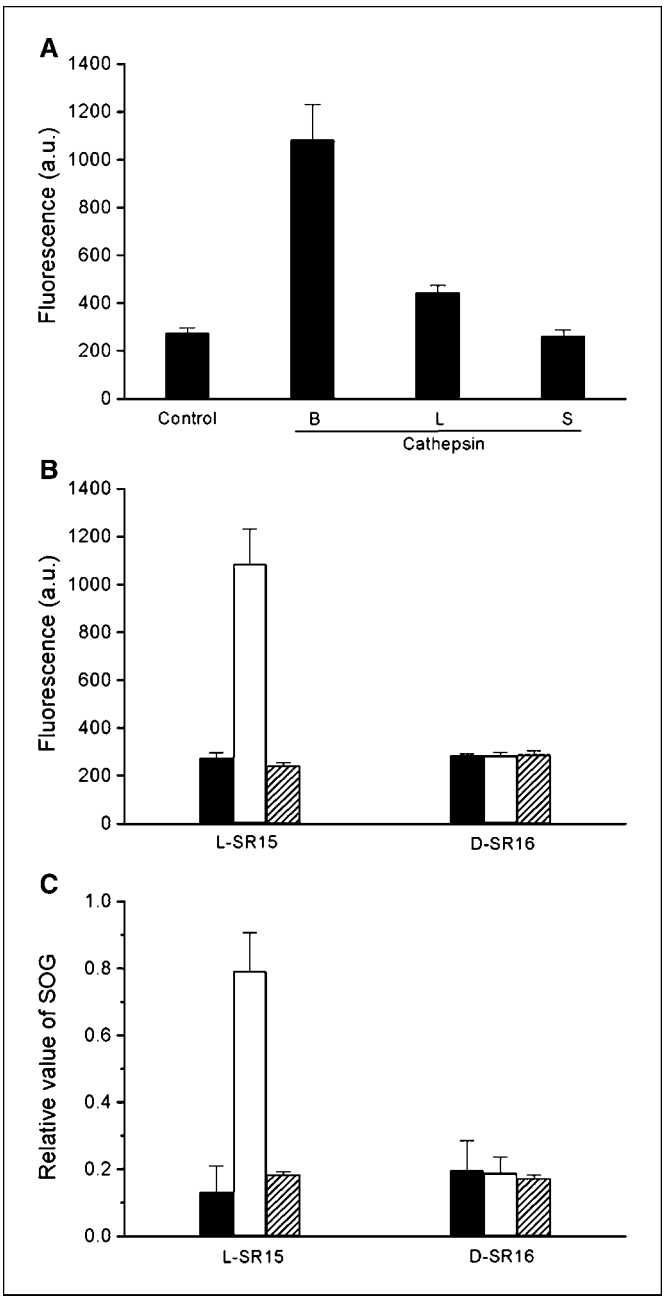


**Figure 2.** Fluorescence activation and single oxygen generation on protease treatment. *A,* fluorescence intensity changes of L-SR15 following treatment with phosphate buffer, cathepsin B, cathepsin L, or cathepsin S. Activation of fluorescence intensity (*B*) and SOG (*C*) of L-SR15 and D-SR16 with phosphate buffer (*black columns*), cathepsin B (*white columns*), and CA-074 inhibitor-pretreated cathepsin B (*striped columns*).

Several experiments were subsequently conducted to corroborate specificity. The cathepsin B inhibitor CA-074 (18) completely inhibited fluorescence recovery on cathepsin B addition (Fig. 2*B*). Furthermore, a poly-D-lysine-based PGC with similar substitution ratio (D-SR16) was also prepared and tested under identical conditions. Similar fluorescence quenching effect (~86% quenching) was observed with the D-backbone; however, no noticeable fluorescence activation occurred on cathepsin B addition. The above results thus confirm that proteolytic degradation is indeed the primary mechanism of fluorescence activation.

SOG of L-SR15 and D-SR16 was subsequently assayed using similar cathepsin B incubation experiments (Fig. 2*C*). In the native state, SOG of L-SR15 was only 13% compared with that of free Ce6 at equimolar concentrations. In the absence of cathepsin B, the buffer containing L-SR15 remained quenched. On cathepsin B treatment, SOG increased up to 79%, a 6-fold increase ($P = 0.0012$). As with the fluorescence experiment, inhibitory effects were observed with CA-074 treatment. As expected, addition of cathepsin B to D-SR16 showed no enhancement in SOG. These results support the hypothesis that not only fluorescence but also SOG can be quenched and selectively recovered on specific protease treatments.

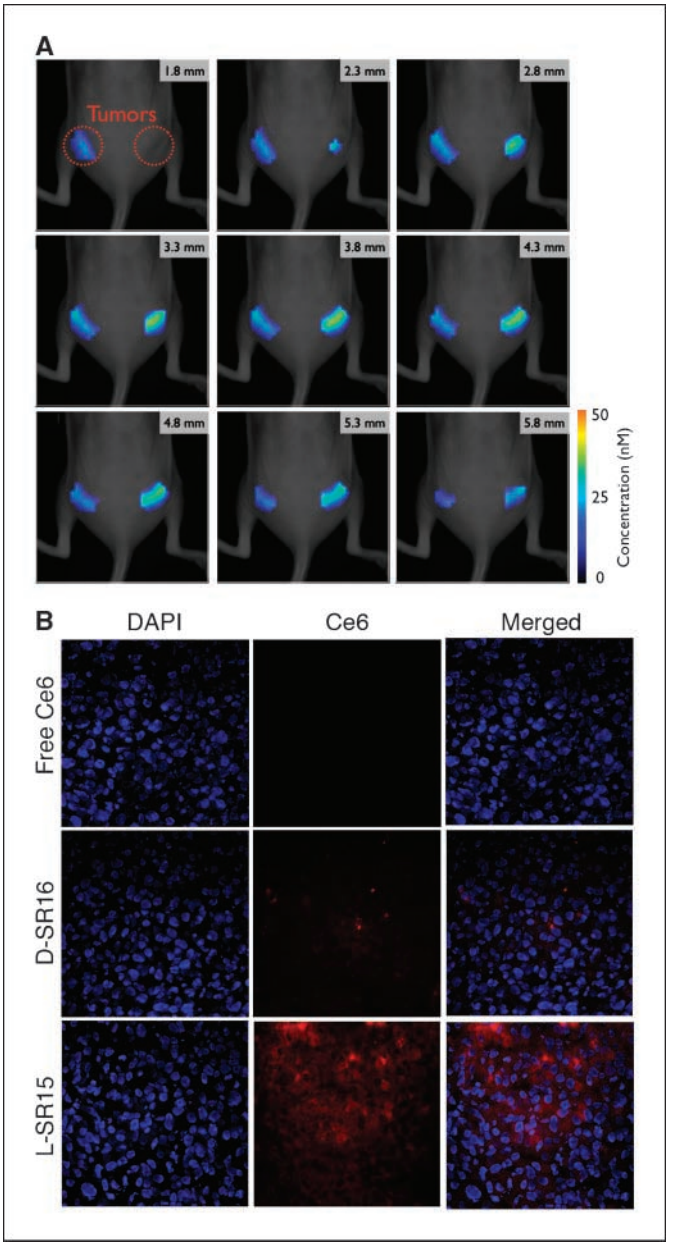


**Figure 3.** *In vivo* activation of PM-PDT. *A,* distribution of imageable Ce6 in bilateral flank tumors. Nine consecutive slices from a three-dimensional fluorescence-mediated tomographic scan. *B,* tumor-bearing mice were injected with free Ce6, D-SR16, or L-SR15. Twenty-four hours later, tumors were collected without light treatment. *Left,* nuclear DAPI staining (*blue*); *middle,* fluorescent signal of Ce6 (*red*); *right,* merged images. Magnification, ×40.

The PM-PDT strategy was next examined *in vivo* using a xenographic tumor model. HT1080 cell line was selected for the animal study because of its high-expressing level of cathepsin B (19). HT1080 human fibrosarcomas were s.c. implanted in both hind legs of mice. After i.v. injection of L-SR15 (0.125 mg Ce6 eq./kg), the fluorescence activation in tumors ($n$ = 6) were clearly imaged using FMT. There was accumulation of L-SR15 in tumor with time, reaching the highest concentration of 17.0 ± 1 nmol/L at 24 hours postinjection (Fig. 3*A*). In a separate set of animals, free Ce6, L-SR15, or D-SR16 (0.125 mg Ce6 eq./kg) was injected i.v.; tumors were collected and sectioned. These animals received no light treatment to preserve fluorescence signal. High fluorescence signal was observed in the animals injected with L-SR15, whereas D-SR16- and Ce6-injected groups showed little or no fluorescence signal (Fig. 3*B*). These results support that L-SR15 is activated in tumors *in vivo* similar as in the previous *in vitro* assays. Merged images showed that the fluorescence of L-SR15 fragments was distributed in cellular cytoplasm but did not localize to the nucleus. On the contrary, D-SR16-treated animals did not show any significant fluorescence in tumors. Although cathepsin B is known as a lysosomal enzyme, it also locates on the surface of cancer cells (20). It explains how the injected L-SR15 conjugate can be efficiently activated in tumors. Another interesting finding was that fluorescence signal of free Ce6 was much lower than that of L-SR15-injected animals. Polymeric drug carriers with PEG grafting, such as PGC conjugate, have shown prolonged blood circulation and higher accumulation in tumors by the EPR effect (12, 21, 22).

To show therapeutic efficacy *in vivo*, L-SR15 or D-SR16 (0.125 mg Ce6 eq./kg) in PBS was injected i.v., and 24 hours later, animals were treated with 650 nm light at a fluence of 10 J/cm$^2$ at an irradiance of 42.1 mW/cm$^2$. Twenty-four hours after the light treatment, tumors were excised, sectioned, and stained for apoptosis. TUNEL staining clearly indicated severe apoptosis in large areas of tumor (Fig. 4*A*). In addition, significant tissue loss was observed in the L-SR15-treated group. In the destructed area, polymorphonuclear cells were also observed, indicating inflammatory responses. In contrast, the D-SR16-injected and light-treated tumor showed no signs of apoptosis (Fig. 4*B*).

Antitumor efficacy of PM-PDT was further evaluated by measuring tumor growth rates. When tumors reached 3 to 5 mm, mice were divided into five groups. Animals were treated with L-SR15 with light illumination (group 1), D-SR16 with light illumination (group 2), L-SR15 without light illumination (group 3), free Ce6 with illumination (group 4), or PBS with light illumination (group 5). In the group that received L-SR15 with light illumination, the mean tumor volume was 46% at day 6 ($P$ = 0.0067) and 54% at day 9 ($P$ = 0.0249) compared with group 2 (Fig. 4*C*). All other treated groups, including L-SR15 without light, free Ce6 with light, and PBS with light, showed no significant antitumor effects. Only the combination of protease-degradable L-SR15 and light illumination resulted in reduced tumor growth rates (Fig. 4*D* and *E*). These data support the hypothesis that tumor-associated proteases can activate PM-PDT agents in tumor.

Prolonged administration of effective concentrations of conventional photosensitizers is usually not possible because of dose-limiting systemic phototoxicities (limited therapeutic window). The combination of the presented PM-PDT and focal light illumination is expected to be an effective treatment with reduced phototoxicity given the quenched state of the native compounds. We show in this study that SOG can be quenched and activated through proteolytic cleavage. Because activation of PM-PDT agents is largely confined to areas of cancer, most unwanted side effects could be prevented. Potentially, the proposed PM-PDT approach could be used as a primary anticancer treatment or as an adjuvant to other therapeutic options. Although its treatment effect is restricted by the limited tissue penetration of light, PDT remains a promising therapy to treat various superficial cancers (e.g., esophageal, gastric, colon, and cervical cancers). Importantly, the proposed strategy is one of the few that allows visualization of the target and local drug concentration before selective therapy (Fig. 3). This therapeutic approach could be used to tailor treatments and avoid unnecessary side effects. We believe that the reported PM-PDT has significant translational potential.

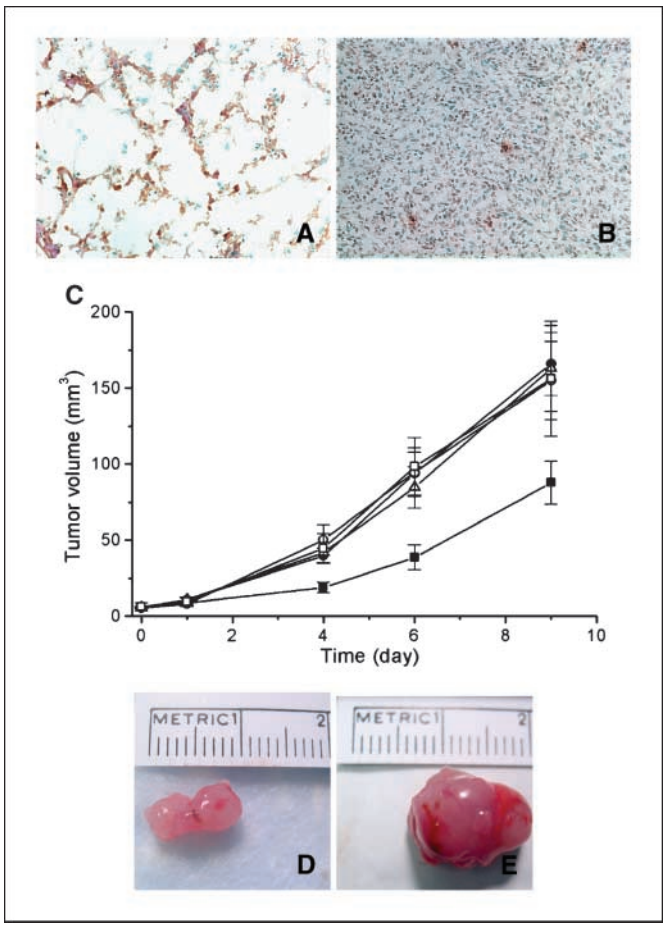


**Figure 4.** *In vivo* PDT. TUNEL staining of (*A*) L-SR15-treated or (*B*) D-SR16-treated tumors 24 hours after light illumination. Magnification, ×20. A 24-hour lag time was applied to allow *in vivo* proteases activation. *C,* tumor size after PM-PDT treatment. *Points,* mean; *bars,* SE. ●, PBS + light illumination ($n$ = 17); ○, free Ce6 + illumination ($n$ = 18); △, D-SR16 + illumination ($n$ = 20); □, L-SR15 without illumination ($n$ = 8); ■, L-SR15 + illumination ($n$ = 19). $n$ = number of tumors involved. *D,* tumor treated with L-SR15 + light. *E,* tumor treated with D-SR16 + light.

## Acknowledgments

Received 2/6/2006; revised 4/12/2006; accepted 5/11/2006.

**Grant support:** NIH grants P50-CA86355, RO1 CA99385, and DOD DC044945.

The costs of publication of this article were defrayed in part by the payment of page charges. This article must therefore be hereby marked *advertisement* in accordance with 18 U.S.C. Section 1734 solely to indicate this fact.

We thank Peter Waterman for the FMT imaging.

## References


1. MacDonald IJ, Dougherty TJ. Basic principles of photodynamic therapy. J Porphyrins Phthalocyanines 2001;5:105–29.
2. Keppler D, Sameni M, Moin K, Mikkelsen T, Diglio CA, Sloane BF. Tumor progression and angiogenesis: cathepsin B & Co. Biochem Cell Biol 1996;74:799–810.
3. Kim J, Yu W, Kovalski K, Ossowski L. Requirement for specific proteases in cancer cell intravasation as revealed by a novel semiquantitative PCR-based assay. Cell 1998;94:353–62.
4. Liaudet E, Derocq D, Rochefort H, Garcia M. Transfected cathepsin D stimulates high density cancer cell growth by inactivating secreted growth inhibitors. Cell Growth Differ 1995;6:1045–52.
5. Garcia M, Platet N, Liaudet E, et al. Biological and clinical significance of cathepsin D in breast cancer metastasis. Stem Cells 1996;14:642–50.
6. DeClerck YA, Mercurio AM, Stack MS, et al. Proteases, extracellular matrix, and cancer: a workshop of the path B study section. Am J Pathol 2004;164:1131–9.
7. Koblinski JE, Ahram M, Sloane BF. Unraveling the role of proteases in cancer. Clin Chim Acta 2000;291:113–35.
8. Lynch CC, Matrisian LM. Matrix metalloproteinases in tumor-host cell communication. Differentiation 2002;70:561–73.
9. Redmond RW, Land EJ, Truscott TG. Aggregation effects on the photophysical properties of porphyrins in relation to mechanisms involved in photodynamic therapy. Adv Exp Med Biol 1985;193:293–302.
10. Damoiseau X, Schuitmaker HJ, Lagerberg JW, Hoebeke M. Increase of the photosensitizing efficiency of the Bacteriochlorin a by liposome-incorporation. J Photochem Photobiol B 2001;60:50–60.
11. Hamblin MR, Miller JL, Rizvi I, Ortel B. Degree of substitution of chlorin e6 on charged poly-L-lysine chains affects their cellular uptake, localization and phototoxicity towards macrophages and cancer cells. J X-Ray Sci Technol 2002;10:139–52.
12. Weissleder R, Tung CH, Mahmood U, Bogdanov A, Jr. *In vivo* imaging of tumors with protease-activated near-infrared fluorescent probes. Nat Biotechnol 1999;17:375–8.
13. Tung CH. Fluorescent peptide probes for *in vivo* diagnostic imaging. Biopolymers 2004;76:391–403.
14. Hartman PE, Hartman Z, Ault KT. Scavenging of singlet molecular oxygen by imidazole compounds: high and sustained activities of carboxy terminal histidine dipeptides and exceptional activity of imidazole-4-acetic acid. Photochem Photobiol 1990;51:59–66.
15. Tomayko MM, Reynolds CP. Determination of subcutaneous tumor size in athymic (nude) mice. Cancer Chemother Pharmacol 1989;24:148–54.
16. Ntziachristos V, Schellenberger EA, Ripoll J, et al. Visualization of antitumor treatment by means of fluorescence molecular tomography with an Annexin V-Cy5.5 conjugate. Proc Natl Acad Sci U S A 2004;101:12294–9.
17. Graves EE, Weissleder R, Ntziachristos V. Fluorescence molecular imaging of small animal tumor models. Curr Mol Med 2004;4:419–30.
18. Yamamoto A, Kaji T, Tomoo K, et al. Crystallization and preliminary X-ray study of the cathepsin B complexed with CA074, a selective inhibitor. J Mol Biol 1992;227:942–4.
19. Hulkower KI, Butler CC, Linebaugh BE, et al. Fluorescent microplate assay for cancer cell-associated cathepsin B. Eur J Biochem 2000;267:4165–70.
20. Cavallo-Medved D, Sloane BF. Cell-surface cathepsin B: understanding its functional significance. Curr Top Dev Biol 2003;54:313–41.
21. Bogdanov AA, Jr., Martin C, Bogdanova AV, Brady TJ, Weissleder R. An adduct of *cis*-diamminedichloroplatinum(II) and poly(ethylene glycol)poly(L-lysine)-succinate: synthesis and cytotoxic properties. Bioconjug Chem 1996;7:144–9.
22. Satchi-Fainaro R, Puder M, Davies JW, et al. Targeting angiogenesis with a conjugate of HPMA copolymer and TNP-470. Nat Med 2004;10:255–61.

# Selective Antitumor Effect of Novel Protease-Mediated Photodynamic Agent

Yongdoo Choi, Ralph Weissleder and Ching-Hsuan Tung

*Cancer Res* 2006;66:7225-7229.